EXPRESS LETTER

Volcanic edifice weakening via devolatilization reactions

Silvio Mollo,[1] Sergio Vinciguerra,[1] Gianluca Iezzi,[1,2] Alessandro Iarocci,[1] Piergiorgio Scarlato,[1] Michael J. Heap[3] and Donald B. Dingwell[3]

[1]*Istituto di Geofisica e Vulcanologia, Via di Vigna Murata* 605*, 00143 Roma, Italy. E-mail: mollo@ingv.it*
[2]*Dipartimento DIGAT, Università G. d'Annunzio, Via dei Vestini 31, 66013 Chieti, Italy*
[3]*Department für Geo- und Umweltwissenschaften, Sektion Mineralogie, Petrologie and Geochemie, LMU, University of Munich, Theresienstr.* 41, 80333 *Munich, Germany*

SUMMARY

Edifice instability, that can result in catastrophic flank collapse, is a fundamental volcanic hazard. The subvolcanic basement can encourage such instability, especially if it is susceptible to mechanical weakening by devolatilization reactions near magmatic temperatures. For this reason, understanding how the physical and chemical properties of representative lithologies deteriorate at high temperatures is potentially highly relevant for volcanic hazard mitigation. This is particularly true for sedimentary rock, commonly found underlying volcanic edifices worldwide, that undergo rapid deterioration even under modest temperatures.

Therefore, here we present the first experimental study of devolatilization reactions, induced by magmatic temperatures, on sedimentary rock comprising a subvolcanic basement. Our results show that, for a marly limestone representative of the basement at Mt Etna, devolatilization reactions, namely the dehydroxylation of clay minerals and the decarbonation of calcium carbonate, result in a dramatic reduction of mechanical strength and seismic velocities. These temperature-driven reactions can promote volcanic instability at stresses much lower than previously estimated.

Key words Phase transitions; Experimental volcanism; Volcanic hazards and risks.

1 INTRODUCTION

The stability of a volcanic edifice is a significant element of volcanic risk assessment. Instability of volcanic flanks can ultimately result in their collapse; indeed, field surveys worldwide have shown them to be common, devastating and not to be overlooked (Siebert 1992). Over the last few decades, volcanic instability has been explained through short-term mechanisms, such as stress triggering in response to dyking (e.g. Bonaccorso *et al.* 2010), and long-term mechanisms such as gravitational volcanic spreading (e.g. van Wyk de Vries & Francis 1997; Borgia *et al.* 2000). A common theme in such mechanisms is that mechanical properties of the sedimentary subvolcanic basement must play a fundamental role. This is interesting on two counts, first, intense heat is provided to the sedimentary substratum by large, long-lived magmatic bodies (e.g. Wohletz *et al.* 1999; Civetta *et al.* 2004; Bonaccorso *et al.* 2010) and circulating hot fluids (Merle *et al.* 2010; Siniscalchi *et al.* 2010). Secondly, the role of devolatilization reactions (i.e. dehydroxylation and decarbonation reactions) in modifying the physical and mechanical properties of the sedimentary substratum, contributing or triggering volcanic instability, has not been experimentally investigated on

representative rock types until now. This poses the question: could these debilitating devolatilization reactions modify the physical and mechanical properties of the sedimentary substratum and therefore contribute to processes driving volcanic instability? However, experimental studies on representative rock types remain absent.

For the purpose of this study, we have selected Mt Etna volcano (Italy) as an example of an active volcano with a thick subvolcanic sedimentary basement (Fig. S1a). Mt Etna represents a prime candidate for our study. First, recent geophysical data (e.g. Lundgren *et al.* 2004; Bonaccorso *et al.* 2010) have not only placed the main region of magma storage within the clay and carbonate rocks of the sedimentary substratum (Fig. S1b), but numerical modelling (e.g. Del Negro *et al.* 2009) has shown that these rocks are at 1000 °C at the contact with the magmatic body and only decrease down to 300 °C at a distance of about 1.5 km (Fig. S1c). Secondly, the edifice overlies a melange of marly clays, marly limestones (MLs) and quartz-arenitic rocks (Catalano *et al.* 2004, Fig. S1), which are believed to enhance the sliding of the structurally unstable eastern flank (Borgia *et al.* 1992), as evidenced by the shallow volcano-tectonic earthquake hypocentres (Patanè *et al.* 2006). Indeed, recent geophysical data at Mt Etna have indicated that two of the proposed

sliding surfaces are present within this weakened sedimentary substratum, at depths of about 1 and 4 km (e.g. Lundgren *et al.* 2004; Battaglia *et al.* 2010).

Here therefore we present the results of an experimental study on the most representative lithology (an ML) of the sedimentary substratum complexity of Mt Etna volcano, where changes in physical and chemical properties are measured at high temperatures. As a basis of comparison we have also investigated two basalts that exist within the overlying pile of lava flows. The results are discussed in terms of thermomechanical weakening and flank instability processes at active volcanoes.

2 MATERIALS AND METHODS

The focus of our study is an ML comprised of ∼75 wt. per cent calcite, ∼15 wt. per cent quartz and ∼10 wt. per cent kaolinite. ML is a basement rock belonging to the Polizzi formation (Sicilide Unit) and outcropping at Mt Etna volcano (see also Catalano *et al.* 2004). The material did not show any significant natural heterogeneity due to the occurrence of altered minerals or pre-existing fractures; however, it is worth noting that ML cannot be considered dry due to the presence of a water-bearing mineral, that is, kaolinite, as characterized by a low-temperature decomposition reaction (see later). The two basalts are an alkali basalt (EB) and a trachybasalt (PB) from lava flows belonging to the shallow part of the volcanic pile. The initial physical properties of EB are also outlined in Heap *et al.* (2011).

Uniaxial compressive tests, acoustic wave velocity measurements, porosity (AccuPyc II 1340 helium pycnometer) and image (Jeol-JSM6500F scanning electron microscope, SEM) analyses were conducted at the 'HP-HT Laboratory of experimental Volcanology and Geophysics' of 'Istituto Nazionale di Geofisica e Vulcanologia' (INGV, Roma). The uniaxial apparatus is equipped with a ceramic furnace and a system for *in situ* *P*-wave velocity (hereinafter termed 'V_p') measurements. Constant strain rate

(0.75 μm s^{-1}) uniaxial compression tests were performed in this setup on cylindrical samples (25 mm diameter by 60 mm length). For ML, temperatures of 25 °C, 300 °C, 600 °C and 760 °C were used to investigate mineral decomposition (Tschegg *et al.* 2009), whereas tests on EB and PB were conducted at 25 °C, 300 °C and 800 °C. Three cores for each sample were tested at the chosen conditions to demonstrate the reproducibility of the data. The experimental temperatures were reached using a constant heating rate of 10 °C min^{-1}, to avoid thermal shock in the samples (Yavuz *et al.* 2010).

Calcimetry analysis was carried out using a Dietrich-Frühling calcimeter at the 'Environmental and Isotope Geochemistry' laboratory of 'Roma Tre' University in Roma (Italy) to measure the amount of calcite dissociated. X-ray powder diffraction pattern (XRPD) was performed at the DIGAT department of Università G. d'Annunzio in Chieti (Italy) to determine the quantitative mineral phase amounts by the Rietveld method. Differential thermal analysis (DTA) was undertaken at the Department für Geo- und Umweltwissenschaften, Sektion Mineralogie, Petrologie and Geochemie of Ludwig Maximilians Universität in Munich (Germany) to investigate the thermal range of mineral reactions.

3 RESULTS AND DISCUSSION

Representative axial stress-strain curves for the ML deformed unconfined at temperatures of 25 °C, 300 °C, 600 °C and 760 °C, are displayed in Fig. 1(a). The deformation behaviour was brittle irrespective of the thermal conditions and all samples failed by axial splitting. However, both the unconfined compressive strength (UCS) and the per cent of strain at brittle failure decreased with increasing temperature. In Fig. 1(b), V_p and UCS values measured for ML are plotted as a function of temperature. Over the entire temperature range (25–760 °C), a drastic decrease from 5.45 to 4.16 km s^{-1} and from ∼167 to ∼89 MPa is observed for V_p and UCS, respectively. In detail, the V_p of the ML samples decreased linearly with increasing temperature from 25 °C to about 700 °C (Fig. 1b). Above 700 °C the
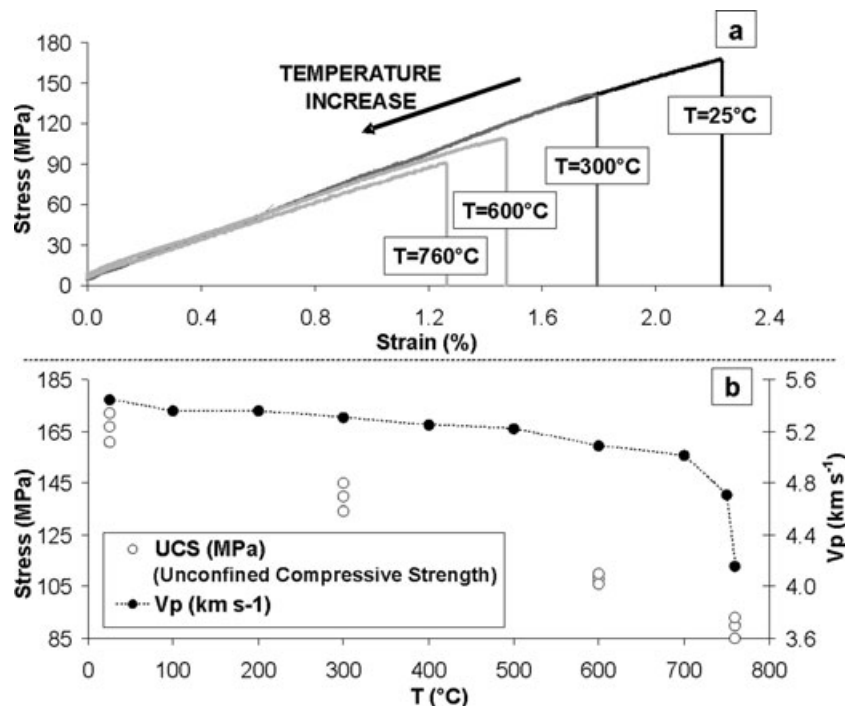
Figure 1. Stress–strain curves for ML (a) and variation of UCS (Unconfined Compressive Strength) and *P*-wave velocity (b) with increasing temperature.
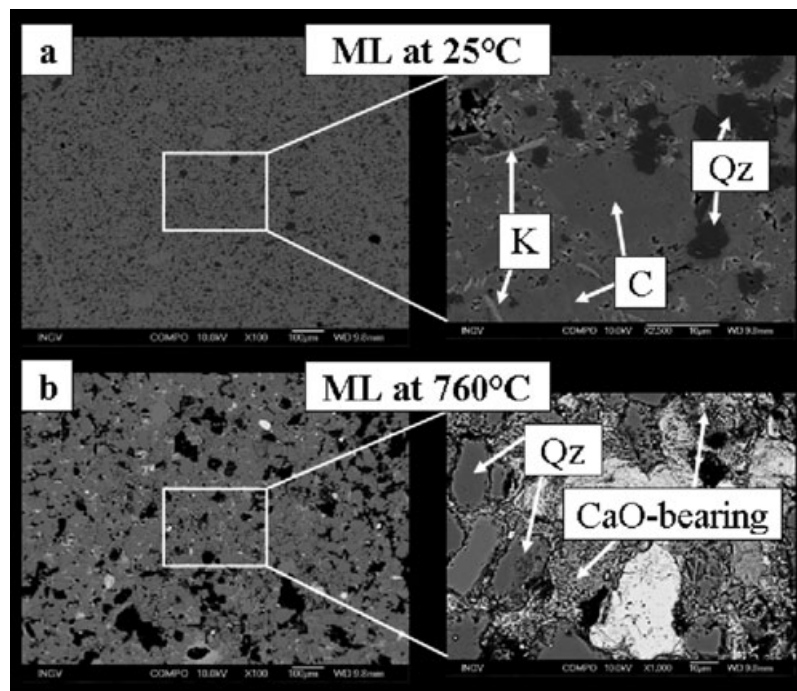
Figure 2. Backscattered SEM images of ML as an as-received sample (a) and heat-treated at 760 °C (b). Cc, calcite; K, kaolinite; Qz, quartz.

velocities decreased substantially. However, the observed decrease in UCS remained linear over the entire temperature range. UCS values decreased by 16, 25 and 47 per cent at temperatures of 300 °C, 600 °C and 760 °C, respectively, from the starting value measured at 25 °C (Fig. 1b).

Combined SEM, calcimetry, porosity, XRPD and DTA analyses were performed on the specimens to track mineral transformations with increasing temperature. In Fig. 2, backscattered SEM images for both the as-collected (25 °C) and heat-treated (760 °C) samples are shown. At 25 °C, the rock texture can be characterized by kaolinite sheets and grains of quartz that are distributed in a dense mosaic of larger calcite crystals (Fig. 2a). Small and sparse inter- and intracrystal cavities are also observed at the scale of the image, explaining the low sample porosity of 2.5 per cent. On the contrary, the sample heat-treated at 760 °C shows that kaolinite crystals have completely disappeared, quartz grains have partly dissolved edges and new CaO-bearing phases appear, showing complex reaction textures (Fig. 2b). Notably, the number and dimension of cavities drastically increase and, consequently, it is somehow surprising the porosity increase is only to 5.4 per cent (i.e. 7.9 per cent from an initial 2.5 per cent).

In Fig. 3, the mineralogical transformations of ML, heat-treated to 300 °C, 600 °C and 760 °C, are illustrated using XRPD data. The Rietveld refinement of data shows that kaolinite decreased from 10 to 5 wt. per cent upon increasing the temperature from 25 °C to 300 °C, and has completely disappeared at 600 °C. This is in response to the progressive dehydroxylation and collapse of the sheet allumino-silicate crystal structure (Girard & Savin 1996). Within the temperature interval of 25–300 °C, the UCS and V_p values decreased from 167 to 140 MPa and from 5.5 to 5.2 km s^{-1}, respectively (Fig. 1). When kaolinite completely disappeared at 600 °C (Fig. 3), thus the UCS and V_p values decreased further to 107 MPa and to 5.1 km s^{-1}, respectively (Fig. 1). In addition, calcite starts to decompose at above 600 °C, releasing carbon dioxide by the following reaction: $CaCO_3 \rightarrow CaO + CO_2$ (Samtani *et al.* 2002).
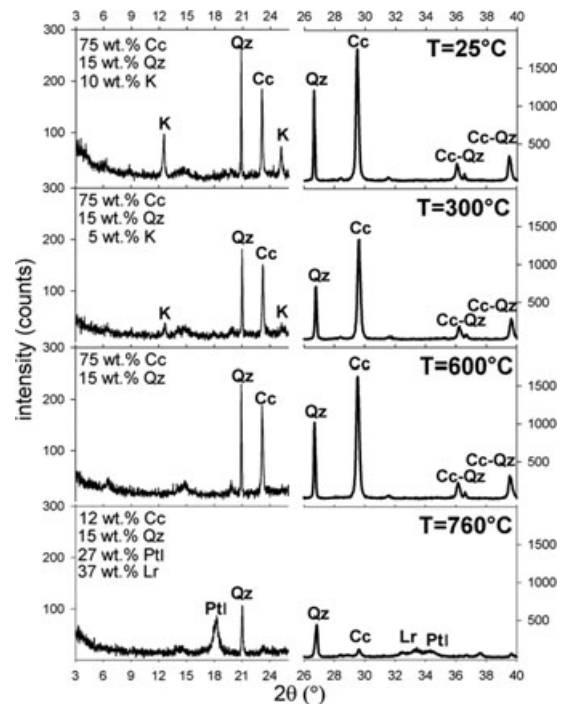
Figure 3. X-ray powder diffraction patterns of ML at 25 °C, 300 °C, 600 °C and 760 °C. Cc, calcite; K, kaolinite; Qz, quartz, Lr, larnite; Pt, portlandite. Note the loss of K below 600 °C and the loss of Cc above 600 °C.

Calcimetry analyses indicate that at 760 °C the amount of calcite is drastically decreased to 12 wt. per cent producing a large amount (∼27 wt. per cent) of CO_2 (Fig. 3). Moreover, the decomposition of calcite in presence of clay minerals produces two CaO-bearing silicates (Fig.3), ∼37 wt. per cent of larnite and ∼27 wt. per cent of portlandite (Tschegg *et al.* 2009). Larnite (Ca_2SiO_4) crystallizes within the CaO-SiO$_2$-CO$_2$ chemical system and it is a common
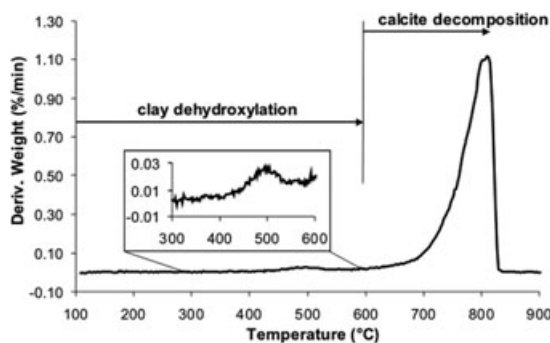
Figure 4. The differential thermal analysis (DTA) plot employed for studying ML decomposition, notably dehydroxilation between $400\,°C$ and $600\,°C$ and decarbonation above $600\,°C$, at a heating rate of $5\,°C\,min^{-1}$ in an atmosphere of argon.

metamorphic mineral of magma-carbonate interaction. In contrast, portlandite is a calcium hydroxide formed by the recombination of CaO with water vapour. However, since the amount of calcite is higher than that of kaolinite, major changes for UCS and V_p values are observed above $600\,°C$ (Fig. 1) corresponding to the temperature necessary to ignite calcite decomposition (Fig. 3).

Hence, two main devolatilization reactions are recognized for ML: (i) in the thermal range from $25\,°C$ to $600°C$, clay dehydroxylation causes the collapse of kaolinite crystal structure and (ii) at temperatures above $600\,°C$, calcite dissociation starts and, consequently, ~64 wt. per cent of new CaO-bearing minerals form at $760\,°C$. In Fig. 1, the DTA plot for the decomposition of ML, illustrates that clay dehydroxylation and calcite decomposition mostly occur from $450\,°C$ to $550\,°C$ and from $700\,°C$ to $800\,°C$, respectively (Fig. 4). It is worth noting that kaolinite and calcite structures contain H_2O and CO_2 amounting to 15 and 44 wt. per cent, respectively; therefore, the release of these volatiles due to devolatilization reactions inevitably produces a material with a significantly disturbed microstructure and a higher porosity (that, in turn, decreases the V_p). It has long been known in rock mechanics that a higher porosity generally translates to a lower UCS (e.g. Palchik 1999; Palchik & Hatzor 2004). Therefore, we can attest that devolatilization reactions are the main processes driving the observed rock weakening in ML.

In contrast, the two basalts, EB and PB, conserve their petrographical features after thermal treatments, even at $800\,°C$. As a result, UCS values and V_p velocities of basalts do not show any significant variation with increasing temperature from $25\,°C$ to $800°C$ (Fig. S2). This behaviour can be explained by the high abundance of mineral phases that, in the applied temperature range, undergo only a very limited thermal expansion (Sack & Ghiorso 1994). Moreover it has been shown that temperatures up to $800\,°C$ are not able to enhance the pre-existing thermal crack damage in some lava flow basalts (Vinciguerra *et al.* 2005; Heap *et al.* 2009).

Studies have shown that large volumes of volcanic sedimentary substrata found beneath volcanoes worldwide can be subjected to the high temperatures used in our experiments (Wohletz *et al.* 1999; Civetta *et al.* 2004; Del Negro *et al.* 2009; Bonaccorso *et al.* 2010; Mollo *et al.* 2010a). Under such thermal conditions, both clay dehydroxylation and calcite decarbonation reactions occur, causing a significant reduction in rock strength (Fig. 1), without any additional tectonic or magmatic force. We contend that this weakening due to devolatilization reactions can result in an increase in volcanic edifice instability. Specifically, pre-existing sliding surfaces found

at appropriate depths can be reactivated at stresses much lower than expected, driving large-scale deformation.

Focussing on Mt Etna, the main region of magma storage, located at 2–5 km of depth (Fig. S1c), is estimated to have a temperature formation from $1200\,°C$ to $1100\,°C$ (Del Gaudio *et al.* 2010; Mollo *et al.* 2010b, 2011) and to induce a thermal gradient from $1000\,°C$ at the contact to $300\,°C$ at a distance of about 1.5 km incorporating a total volume of about $9\,km^3$ of sedimentary substratum (Del Negro *et al.* 2009; Bonaccorso *et al.* 2010). Furthermore, this source region should not be regarded as stationary, but as part of a dynamic dyke intrusive complex (Fig. S1c) that can reach, and therefore weaken, fresh, unaltered sedimentary material; thus further increasing volcanic instability. Recent geophysical data at Mt Etna have indicated that two of the proposed sliding surfaces are present within this weakened sedimentary substratum (Lundgrun *et al.* 2004; Battaglia *et al.* 2010). Therefore, the shallow pile of the mechanically stronger lava flow deposits can essentially 'float' on the weaker sedimentary layers, accommodating the stress through brittle failure, as demonstrated by the intense shallow seismic swarms at Mt Etna volcano (Patanè *et al.* 2006).

From a seismological and geochemical monitoring point of view, further implications can be discussed. For example, the sharp decrease of seismic velocities observed during our experiments, correlates well with the anomalously low seismic velocities recorded in the subvolcanic basement at Mt Etna (Patanè *et al.* 2006), and other active volcanoes worldwide (e.g. Molina *et al.* 2005 and references therein). Our experimental data open new perspectives, since low seismic velocities can be related to weakened lithologies that drive strain localization along sliding surfaces. Such results can thus allow, in perspective, a much higher reliability of flank instability and/or collapse forecast, with a strong impact on hazard mitigation. Furthermore, the decarbonation process, occurring between $600\,°C$ and $800\,°C$ in the sedimentary carbonate layers, can also contribute to the anomalously high CO_2 emissions measured before volcanic eruptions (Allard *et al.* 2006).

5 CONCLUSIONS

We have reported, for the first time, experimental data on the thermochemical reactions and mineralogical transformations induced by magmatic activity within the sedimentary substratum of active volcanoes. An ML, representative of the sedimentary basement of Mt Etna volcano, was heated to magmatic temperatures and loaded to failure in a uniaxial apparatus, while measuring *in situ* elastic-wave velocities. The weakening of the ML via devolatilization reactions (i.e. clay dehydroxylation and calcite decarbonation) resulted in a significant decrease in both UCS and V_p velocity. In contrast, no temperature-induced reactions were initiated in the tested igneous lithologies and consequently no change in their physical properties was observed.

Our study has shown that devolatilization reactions and mineralogical transformations within a sedimentary substratum (i) can promote volcanic edifice instability at stresses much lower than expected, (ii) can explain anomalously low seismic velocities zones and (iii) can contribute to the anomalously high CO_2 emissions measured before volcanic eruptions.

REFERENCES

Allard, P. *et al*., 2006. Mount Etna 1993–2005: anatomy of an evolving eruptive cycle, *Earth Sci. Rev.,* **78,** 85–114.

Battaglia, M. *et al*., 2010. Dike emplacement and flank instability at Mount Etna: constraints from a poro-elastic-model of flank collapse, *J. Volc. Geotherm. Res.,* **199,** 153–164.

Bonaccorso, A. *et al*., 2010. Dike deflection modelling for inferring magma pressure and withdrawal, with application to Etna 2001 case, *Earth planet. Sci. Lett.,* **293,** 121–129.

Borgia, A., Ferrari, L. & Pasquarè G., 1992. Importance of gravitational spreading in the tectonic and volcanic evolution of Mount Etna, *Nature,* **357,** 231–235.

Borgia, A., Delaney, P.T. & Denlinger, R.P., 2000. Spreading volcanoes, *Annu. Rev. Earth planet. Sci.,* **28,** 539–570.

Catalano, S., Torrisi, S. & Ferlito C., 2004. The relationship between late Quaternary deformation and volcanism of Mt. Etna (eastern Sicily): new evidence from the sedimentary substratum in the Catania region, *J. Volc. Geotherm. Res.,* **132,** 311–334.

Civetta, L. *et al*., 2004. Thermal and geochemical constraints on the 'deep' magmatic structure of Mt. Vesuvius, *J. Volc. Geotherm. Res.,* **133,** 1–12.

Del Gaudio P. *et al*., 2010. Cooling rate-induced differentiation in anhydrous and hydrous basalts at 500 MPa: implications for the storage and transport of magmas in dikes, *Chem. Geol.,* **270,** 164–178.

Del Negro, C., Currenti, G. & Scandura, D., 2009. Temperature-dependent viscoelastic modeling of ground deformation: application to Etna volcano during the 1993–1997 inflation period, *Phys. Earth planet. Inter.,* **172,** 299–309.

Girard, J.-P. & Savin, S.M., 1996. Intracrystalline fractionation of oxygen isotopes between hydroxyl and non hydroxyl sites in kaolinite measured by thermal dehydroxylation and partial fluorination, *Geochim. cosmochim. Acta.,* **60,** 469–486.

Heap, M.J., Vinciguerra, S. & Meredith, P.G., 2009. The evolution of elastic moduli with increasing crack damage during cyclic stressing of a basalt from Mt. Etna, *Tectonophysics,* **471,** 153–160.

Heap, M.J. *et al*., 2011. Brittle creep in basalt and its application to time-dependent volcano deformation, *Earth planet. Sci. Lett.,* **307,** 71–82, doi:10.1016/j.epsl.2011.04.035.

Lundgren, P. *et al*., 2004. Gravity and magma induced spreading of Mount Etna volcano revealed by satellite radar interferometry, *Geophys. Res. Lett.,* **31,** L04602, doi:10.1029/2003GL018736.

Merle, O., Barde-Cabusson, S. & van Wyk de Vries, B., 2010. Hydrothermal calderas, *Bull. Volcanol.,* **72,** 131–147.

Molina, I. *et al*., 2005. Three-dimensional P-wave velocity structure of Tungurahua Volcano, Ecuador, *J. Volc. Geotherm. Res.,* **147,** 144–156.

Mollo, S. *et al*., 2010a. Carbonate assimilation in magmas: a reappraisal based on experimental petrology, *Lithos,* **114,** 503–514.

Mollo S. *et al*., 2010b. Dependence of clinopyroxene composition on cooling rate in basaltic magmas: implications for thermobarometry, *Lithos,* **118,** 302–312.

Mollo, S. *et al*., 2011. Plagioclase-melt (dis)equilibrium due to cooling dynamics: implications for thermometry, barometry and hygrometry, *Lithos,* **125,** 221–235, doi:10.1016/j.lithos.2011.02.008.

Palchik, V., 1999. Influence of porosity and elastic modulus on uniaxial compressive strength in soft brittle porous sandstones, *Rock Mech. Rock Eng.,* **32,** 303–309.

Palchik, V. & Hatzor, Y.H., 2004. The influence of porosity on tensile and compressive strength of porous chalks, *Rock Mech. Rock Eng.,* **37,** 331–341.

Patanè, D. *et al*., 2006. Time-resolved seismic tomography detects magma intrusions at Mount Etna, *Science,* **313,** 821–823.

Sack, R.O. & Ghiorso, M.S., 1994. Thermodynamics of multicomponent pyroxenes: I. Formulation of a general model, *Contrib. Mineral. Petrol.,* **116,** 277–286.

Samtani, M., Dollimore, D. & Alexander, K.S., 2002. Comparison of dolomite decomposition kinetics with related carbonates and the effect of procedural variables on its kinetic parameters, *Thermochim Acta,* **392–393**, 135–145, doi:10.1016/S0040-6031(02)00094-1.

Siebert, L., 1992. Volcano hazards-threats from debris avalanches, *Nature,* **356,** 658–659.

Siniscalchi, A. *et al*. 2010. Insights into fluid circulation across the Pernicana Fault (Mt. Enta, Italy) and implications for flank instability, *J. Volc. Geotherm. Res.,* **193,** 137–142.

Tibaldi, A. & Groppelli, G., 2002. Volcano-tectonic activity along structures of the unstable NE flank of Mt. Etna (Italy) and their possible origin, *J. Volcanol. Geotherm. Res.,* **115,** 277–302.

Tschegg, C., Ntaflos, T. & Hein I., 2009. Thermally triggered two-stage reaction of carbonates and clay during ceramic firing: a case study on Bronze Age Cypriot ceramics, *Appl. Clay Sci.,* **43,** 69–78.

Vinciguerra, S. *et al*., 2005. Relating seismic velocities, thermal cracking and permeability in Mt. Etna and Iceland basalts, *Int. J. Rock Mech. Min. Sci.,* **42,** 900–910.

van Wyk de Vries, B. & Borgia A., 1996. The role of basement in volcano deformation, *Geol. Soc. London Spec. Pub.,* **110,** 95–110.

van Wyk de Vries, B. & Francis P.W., 1997. Catastrophic collapse at stratovolcanoes induced by gradual volcano spreading, *Nature,* **387,** 387–390.

Wohletz, K., Civetta, L. & Orsi, G., 1999. Thermal evolution of the Phlegraean magmatic system, *J. Volc. Geotherm. Res.,* **91,** 381–414.

Yavuz, H., Demirdag S. & Caran, S., 2010. Thermal effect on the physical properties of carbonate rocks, *Int. J. Rock Mech. Min. Sci.,* **47,** 94–103.

SUPPORTING INFORMATION

Additional Supporting Information may be found in the online version of this article:

Figure S1. Tectonic sketch map of eastern Sicily (a). Key: (1) Late Quaternary volcanics (Mt Etna and Aeolian Islands); (2) Plio-Pleistocene volcanics (Hyblean Plateau); (3) Hyblean Plateau sequences; (4) Gela-Catania Foredeep deposits: (a) Middle-Upper Pleistocene deposits on allochthonous units, (b) Quaternary deposits on the Hyblean sequences; (5) Neogene-Quaternary accretionary wedge units; (6) Maghrebian Thrust Belt units; (7) Calabrian arc units; (8) Front of allochthonous units; (9) Main strike-slip faults; (10) Main thrust; (11) Main Quaternary normal faults. Schematic sketch section of the NE flank of Mt Etna (b). Thermal gradients at Mt Etna volcano (c). Figures redrawn from Tibaldi & Groppelli (2002), Catalano *et al.* (2004) and Bonaccorso *et al.* (2010).

Figure S2. Variations of UCS and *P*-wave velocity of EB (a) and PB (b) basaltic samples with increasing temperature.

Please note: Wiley-Blackwell are not responsible for the content or functionality of any supporting materials supplied by the authors. Any queries (other than missing material) should be directed to the corresponding author for the article.